Positronium formation and diffusion in crystalline and amorphous ice using a variable-energy positron beam

M. Eldrup*
Chemistry Department, Risø National Laboratory, DK-4000 Roskilde, Denmark

A. Vehanen
Laboratory of Physics, Helsinki University of Technology, SF-02150 Espoo 15, Finland

Peter J. Schultz
Department of Physics, The University of Western Ontario, London, Ontario, Canada N6A 3K7

K. G. Lynn
Physics Department, Brookhaven National Laboratory, Upton, New York 11973
(Received 2 May 1985)

The behavior of positrons in crystalline and amorphous ice has been studied with a beam of monoenergetic positrons with incident energies 0—4.5 keV. Positronium (Ps) is formed in the bulk ice and diffuses until it annihilates or escapes from the surface. Measurements were carried out on the fraction of ortho-Ps leaving the surface and of the Doppler broadening of the 511-keV γ annihilation line. For incident energies 0—60 eV the Ps formation probability shows large variations. These variations are associated with Ps formation in the so-called Ore gaps and reflect the electronic structure of ice as demonstrated by Monte Carlo simulations of the positron slowing-down process. At higher energies, up to about 1 keV, the total Ps yield increases from about 50 to 75 %, which is attributed to Ps formation via spur processes. A large difference is found between the Ps diffusion coefficient in crystalline ice (about 0.2 cm^2/sec) and in amorphous ice (roughly 10^{-3} cm^2/sec). From the red shift of the 511-keV annihilation line the Ps work function (affinity) in the crystalline ice is estimated to be -2 ± 1 eV. Evidence for low-energy-positron diffraction in the crystalline ice is found with scattered intensities higher than 25%. Sputtering of the crystalline ice creates surface damage which strongly reduces the yield of Ps escaping the surface. Cavities of average diameter larger than about 17 Å are found in the as-grown amorphous ice. They anneal out at about 100 K, which is below the crystallization temperature of about 135 K.

I. INTRODUCTION

Conventional positron-annihilation experiments make use of positron-emitting isotopes which have maximum energies from 0.5 to 1.5 MeV. In metals such positrons penetrate of the order of 10—100 μm. Hence, the experiments normally give information about bulk properties. For recent reviews of the field, see Refs. 1—4.

In recent years a new technique, the low-energy-positron beam, has been developed. (See, e.g., Refs. 5—8). Here the energetic positrons from a radioactive source are first moderated to thermal energies in a metal crystal, after which a fraction of them (3×10^{-3}—10^{-4}) leaves the surface of the moderator with a well-defined energy (a few electron volts) equal to the negative of the positron work function of the metal.[7] These positrons may then be accelerated, thus constituting a variable-energy beam of monoenergetic positrons.[7,9] Such beams have been intensively used in studies of atomic physics[5,7] and of surface and near-surface phenomena in solids, in particular metals.[6—8] The latter investigations have mainly been dealing with positron-surface interactions, positron diffusion, and positron trapping at defects in the bulk and at surface and interfacial layers.[6—8,10,11]

The aim of the present work has been to study the interaction of low-energy positrons and Ps with a molecular solid. As a first example we have chosen ice which has been extensively investigated both by conventional positron-annihilation methods[12,13] as well as by many other techniques.[14] Unlike in metals, positrons injected into most molecular solids have a nonzero probability of forming Ps in the bulk of the material. The process by which Ps is formed in condensed molecular materials has been a matter of much debate.[15—19] According to the Ore model of Ps formation,[15] which is recognized as being valid for low-density gases,[19] the positron during its slowing down picks off an electron from a molecule with which it simultaneously forms Ps. For energies below $E_L = I - 6.8$ eV, where I is the lowest ionization energy and 6.8 eV is the Ps binding energy in vacuum, this process is not energetically possible. Above an energy $E_U \sim I$ the model predicts a reduction of the yield of stable Ps, because the Ps formation process must complete with rapid slowing down of the positron by excitation and ionization. A Ps atom formed by a positron of energy above E_U may also split up again, thus reducing the yield of stable Ps. The energy range $E_L \leq E \lesssim E_U$ is the so-called Ore gap in gases.[15]

 ©1985 The American Physical Society

The spur model of Ps formation,[18,19] which has successfully accounted for numerous experimental observations, describes the Ps formation as a two-step process. At the end of its slowing down the positron first loses the last part of its kinetic energy (normally assumed about 30—100 eV) by creating a spur[18,19] (a region containing reactive species, i.e., electrons, ions, and radicals as well as the positron). After these species have thermalized the positron may combine with an excess electron in the spur to form Ps (in competition with other processes). Thus, since the characteristic positron energies in the two models were expected to be different, it seemed possible to differentiate between the two models by measurements of the Ps yield as a function of the positron energy.

Another important property which may be determined with low-energy-positron experiments is the Ps diffusion coefficient. Ps diffusion coefficients have been published for only a few insulators,[15,20] and their values scatter over several orders of magnitude. The reason for this scatter may be that most of these measurements were made on amorphous or strongly defected crystalline samples (powders) which were not always well characterized.[15] Hence, there is almost no data on Ps diffusion in crystalline solids, and theoretical discussions of the subject are few.[15] This is so despite the fact that Ps is one of the few neutral light particles whose diffusion in a solid may be studied, and as such of general interest. Also, for other investigations, e.g., of defects in molecular crystals[13] it would be very valuable to know the Ps diffusion coefficient as well as its temperature dependence. Slow-positron measurements are a relatively direct method of establishing Ps diffusion coefficients. Like positrons in metals, Ps formed in an insulator may diffuse back to the surface and escape. By measuring the fraction of Ps that escapes through the surface for different incident positron energies (and hence different depths of Ps formation), the Ps diffusion coefficient is determined.

Further information about the behavior of the positron (or Ps) can be obtained from measurements of the Doppler broadening of the 511-keV annihilation radiation line. We use this method to estimate the kinetic energy with which Ps leaves the surface (i.e., the negative Ps affinity).

In the present work both crystalline and amorphous ice have been studied using positrons of energies in the range 0—4.5 keV. Both the yield of 3γ annihilations and the Doppler broadening of the annihilation line shape were measured over the temperature range 45—150 K. A brief account of some of these results has been given previously.[21] This paper gives a more complete report of the whole work. The main results obtained were a determination of the Ps diffusion coefficient, and a demonstration that in the present experiments one contribution to the total Ps yield comes from positrons with typical Ore gap energies, and another contribution, due to spur processes, from positrons with initial energies of several hundred eV. Furthermore, crystalline and amorphous ice gave strikingly different results, with strong evidence for large cavities in the as-grown amorphous solid. Damaging the crystalline ice surface by ion sputtering strongly influenced both the Ps formation and diffusion. Finally, the Ps affinity to the crystalline ice has been roughly estimated.

The paper has been divided into the following sections. The next section gives the experimental details. Section III contains some theoretical considerations and describes the data analysis. In Sec. IV the results are presented and discussed, and a summary and conclusion is contained in Sec. V. Two appendixes give details on Monte Carlo simulations of positron slowing down and Ps formation (Appendix A) and simulations of Doppler broadening curves (Appendix B).

II. EXPERIMENTAL DETAILS

The low-energy-positron beam used for the present experiments was the one described by Lynn and Lutz,[9] in which the positrons after moderation in the source end of the machine are magnetically guided to the target chamber. The beam has a diameter of about 6 mm and is essentially monoenergetic (width ≤ 1 eV) with energies in the range 0—4.5 keV. The positrons are transported from the source end at a fixed energy of 15 or 25 eV. The energy with which the positrons hit the sample is then determined by the sample potential. For low-energy measurements ($0 < E \lesssim 1000$ eV) the sample potential was ramped at a frequency of about 0.1 sec^{-1} and data was collected in a multichannel analyzer in the multiscaling mode. For high-energy measurements ($0 < E < 4.5$ keV) the sample bias was fixed for a certain measuring time, data being collected by two scalars (see below) and subsequently stored in a computer, before a new sample bias was chosen. The sample biases were normally chosen in a fixed random order. For both types of measuring procedures a total spectrum was recorded in 1—2 hours.

Measurements of the energy spectrum of the annihilation photons emerging from the sample and its vicinity were made with an intrinsic Ge detector which has a full width at half maximum (FWHM) resolution of $\simeq 1.45$ keV at 514 keV. The detector was placed on the beam axis behind the sample. Two types of measurements were carried out. In one type the number of counts (P) in the 511-keV photopeak (500—520 keV) as well as the total number of counts in the spectrum (T) were recorded to be used for the determination of the 3γ yield. In the other type of 511-keV annihilation line was recorded in 78 channels of a multichannel analyzer for determination of the Doppler broadening of the line. The energy dispersion was 187.6 eV per channel, and the centroid was maintained by a digital stabilizer. The shape of the 511-keV line was characterized by two parameters, S and W. S was the area between channels 34 and 44, W the sum of the areas between channels 10 and 29, and 49 and 68, both S and W being normalized to the total area within the 78 channels.

The ice samples were made by depositing water vapor onto a cold Cd single-crystal substrate. The Cd crystal was mounted on the cold stage of a closed-cycle He refrigerator, electrically isolated from ground (Fig. 1). The sample could be cooled to about 45 K. The sample temperature was controlled by simultaneous cooling and electrical heating, or the sample was heated by switching off

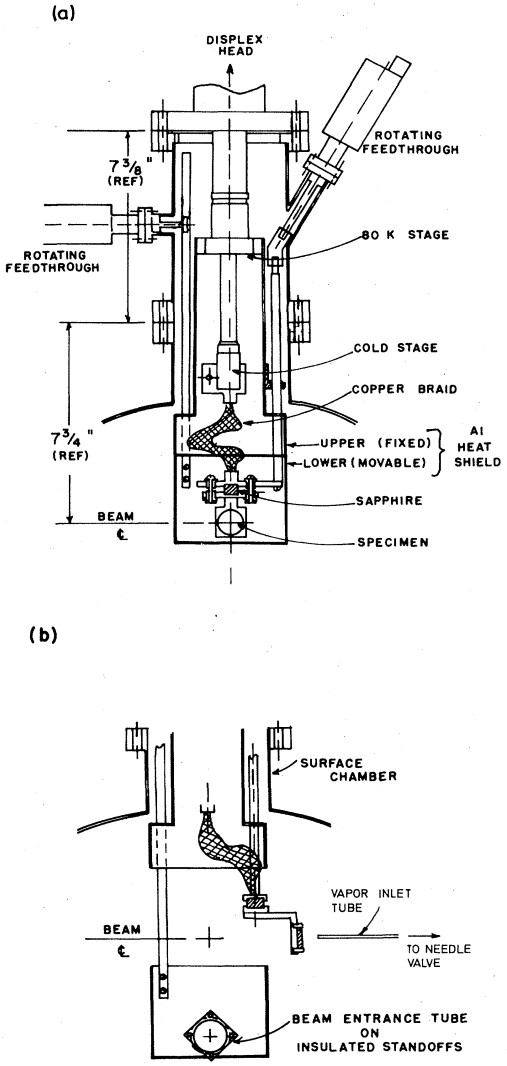

FIG. 1. (a) shows the sample in the measuring position in the UHV target chamber. The Cd crystal (specimen) on which the ice is deposited is thermally connected to the He refrigerator (Displex) through a sapphire (electrically insulating) and a flexible copper braid. The specimen is surrounded (except for the beam entrance hole) by a heat shield. The bottom part of this can be lowered to allow the specimen to be turned in front of the vapor inlet tube for water-vapor deposition (b).

the refrigerator (recording data during the slow warm-up). The temperature was measured by Chromel-Alumel thermocouples and a Pt resistor thermometer. The sample could be turned away from the beam positron to make possible ion bombardment from a sputtering gun and water-vapor deposition. For the latter the Cd crystal was positioned about 1 cm in front of the water-vapor inlet, a 3-mm-diam stainless-steel tube [Fig. 1(b)]. Before deposition the pressure in the target chamber was about 10^{-9} torr. The deposition rate was determined by a leak valve separating the tube and a water reservoir. Triple-distilled water was used which was degassed by several freeze-thaw cycles and subsequent pumping on the vigorously stirred liquid water.

A number of investigations have been carried out to study the structure of solid ice formed by vapor deposition,[14] most recently by Rice and co-workers with the aim of producing amorphous ice.[22] Based on the results of these studies we have grown samples of crystalline ice [mainly ice Ic (cubic), maybe with a small admixture of ice Ih (hexagonal)] by deposition at about 150 K and at a rate of roughly 0.5 μm/min (for an estimated sample size of 1 cm^2), while amorphous ice was created by a roughly ten times lower deposition rate onto a 45—50-K cold surface. The sample thicknesses were estimated at roughly 10 μm. This thickness ensures that the positrons stop in the ice and do not penetrate into the Cd substrate.

Measurements were carried out in the range 45—150 K. The upper temperature was limited by the sublimation of the sample at higher temperatures.

A problem anticipated to arise during the experiments was that of sample charging, because the positrons remove electrons from the sample. Heavy charging of the sample may lead to an ill-defined sample potential, and hence a large uncertainty in the positron incident energy. In order to neutralize the positive-charge buildup an electron flood gun was installed which could flood the sample with electrons of 0—2 eV. However, the sample charging by the positrons turned out to be less severe than was anticipated. Several scans were possible without appreciable charging of the sample, especially at the highest temperatures.

III. THEORETICAL CONSIDERATIONS AND DATA ANALYSIS

In many insulators Ps formation may take place in the bulk of the material. Before Ps annihilates it may be captured by defects[13] (in solids) or undergo chemical reactions with some of the molecules.[23] If the Ps atoms are formed sufficiently close to the surface they may also diffuse to and escape through the surface. Annihilation of para-Ps (p-Ps, singlet state) in the bulk takes place with the emission of two γ quanta and with a mean lifetime close to the vacuum value of 125 psec. Annihilation of ortho-Ps (o-Ps, triplet state) takes place mainly via the so-called pick-off process[23] by which the positron annihilates with one of the electrons of the medium into two γ quanta, while only a very small fraction undergoes intrinsic annihilation into three γ quanta. Typical lifetimes for o-Ps annihilation in the solid are a few nsec, which is much shorter than the vacuum (intrinsic) lifetime of 142 nsec against 3γ decay.

Positrons (not forming Ps) may also diffuse to the surface of an insulator. However, thermalized positrons at the surface of a molecular solid cannot normally form Ps because the electron ionization energy of the medium is too high for it to be energetically possible. This is contrary to the situation in most metals. The formation process will be discussed further in Sec. IV. The Ps escaping through the surface into the vacuum has, therefore, normally been formed in the bulk and diffused back to the surface. The average Ps diffusion length is given by $L_i=(D_{\mathrm{Ps}}\tau_i)^{1/2}$, where D_{Ps} is the Ps diffusion coefficient

and τ_i is the o-Ps ($i=o$) or the p-Ps ($i=p$) lifetime. Since p-Ps usually lives much shorter than does o-Ps, $L_p < L_o$. Hence, if o-Ps and p-Ps are formed in the ratio of 3:1 at a distance from the surface,[15] this ratio is higher than 3 for the Ps which escapes into vacuum.

The calculation of the fraction, f, of positrons which annihilate from an o-Ps vacuum state is analogous to that used for metals.[7,24] It is based on the ratio $R_f=(T_f-P_f)/P_f$, where T_f is the total number of counts in the γ-ray spectrum and P_f is the number of counts in the 511-keV photopeak (500—520 keV). f is then given by

$$f=\frac{3}{4}\left[1+\frac{P_{75}}{P_0}\frac{R_{75}-R_f}{R_f-R_0}\right]^{-1}, \tag{1}$$

where subscripts 0 and 75 refer to situations where 0% or 75% of the implanted positrons escape the surface as o-Ps. Equation (1) differs slightly from the similar formula used previously,[6–8,24,25] since in the present case f only represents the fraction of 3γ decays (i.e., only o-Ps), and hence $0\leq f\leq 0.75$. (Previously,[24] f was normalized to include also p-Ps, and thus $0\leq f\leq 1.0$). As discussed in detail in Refs. 24 and 26, the accuracy with which f can be determined depends on the accuracy with which the ratio P_{75}/P_0, and the limiting values, R_0 and R_{75}, can be estimated. We used the following parameters in the analysis of the data: $P_{75}/P_0=0.4$, $R_0=5.9$, $R_{75}=13.0$, as deduced from previous measurements.

Positrons that do not form Ps and hence annihilate as "free" positrons (in insulators or in metals) have a small probability ($\frac{1}{372}$) of 3γ decay.[23] With the parameters mentioned above, Eq. (1) incorporates these bulk 3γ decays from "free positrons" in such a way that the calculated f represents only those 3γ decays which originate from o-Ps in vacuum. When Ps also forms in the bulk of the sample one normally expects an increase of the total 3γ annihilation probability. In crystalline ice the o-Ps lifetime is 0.7 nsec,[12] and hence the average probability of 3γ decay for those positrons forming Ps is $\frac{3}{4}\times 0.7/142$, which only exceeds $\frac{1}{372}$ by 1.1×10^{-3}. Thus, for ice the correction to f from Ps formation in the bulk is at most about 0.1% and is therefore ignored. However, for other molecular substances with o-Ps lifetimes of several nsec it may be important. In such cases the parameters R_0 and P_{75}/P_0 should be determined directly using the molecular sample, and not by using a metal sample in its place.

Values of f as a function of positron incident energy E were measured mainly in two different energy intervals, viz. $0<E<65$ eV and $0<E<4.5$ keV. Figure 2 shows two typical low-energy curves, (b) for a freshly grown crystalline ice sample, and (c) for a sample which had been charged to a couple of volts by the beam (Fig. 1 in Ref. 21). Figure 2(a) shows the measured total (T_f) number of counts for Fig. 2(b). The positron incident energy was varied by changing the target potential from 29.4 to -38.2 V, keeping the Cu converter at 25.1 V. $E=0$ in Fig. 2(b) was defined by the beam onset (the steep rise in T_f) which happened at a sample potential of 26.0 V, i.e., for a nominal positron incident energy of -0.9 eV. This deviation from zero is attributed to the contact potential

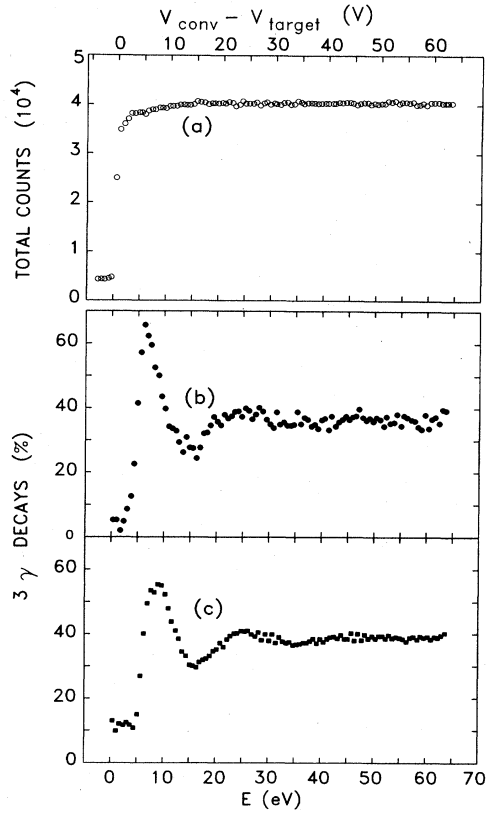

FIG. 2. (a) shows the total number of counts, T_f, and (b) the fraction of 3γ decays, f, as a function of positron incident energy, E, for a freshly grown ice crystal. The sharp rise in T_f clearly shows the "beam onset" which defines $E=0$ eV (equivalent to a nominal positron energy of $V_{\text{conv}}-V_{\text{target}}=-0.9$ eV, upper scale). (c) is equivalent to (b), but obtained with better statistical accuracy and for a sample which had been nonuniformly charged a couple of volts by the beam. This charging introduces a shift and a broadening (and hence lower peak value), especially of the peak at 6 eV. (c) is the same as shown in Fig. 1 in Ref. 21.

difference between the slow-positron converter and the target minus the positron work function of the Cu converter.

In Fig. 3 we show typical curves $f(E)$ for the high-energy range above the oscillatory behavior of Fig. 2. Small differences between different samples were observed, but the main characteristics were the same. As discussed in Ref. 21, the initial increase in f with E is ascribed to an increase in the yield of Ps formed in the ice. The decrease of f at higher energies is resulting from a decrease of the fraction of Ps which diffuses back to the surface. The high-energy (50 eV $<E<$ 4.5 keV) curves were fitted with a model:

$$f=p(E)d_o(E)=p(E)/[1+(E/E_o)^n], \tag{2}$$

where

$$p(E)=p_{\max}+(p_0-p_{\max})\exp[-\tfrac{1}{2}(E/E_1)^\beta] \tag{3}$$

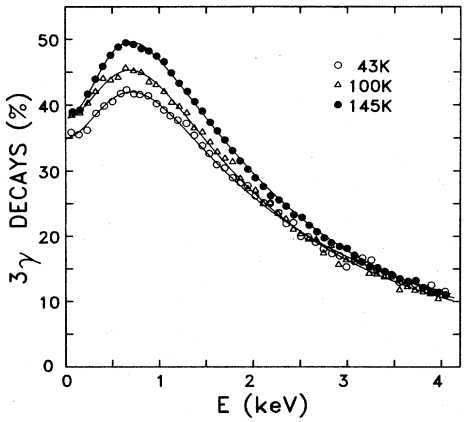

FIG. 3. The 3γ yield, f, as a function of positron incident energy at three different temperatures for crystal 1. The increase in f results from an increase in the Ps formation probability, while the decrease is due to the finite diffusion length of o-Ps before annihilation. The curves are fits of Eq. (2) to the data.

is an empirical expression chosen to describe the increase of the o-Ps yield with energy from p_0 at $E\sim 50$ eV up to $p_{\max}$ for large E (see Sec. IV). The function $d_o(E)$, which gives the fraction of o-Ps that diffuses back to the surface, was derived[27] from a one-dimensional diffusion model. The shapes of typical curves, d_o, p, and f, are shown in Fig. 4. In Eq. (2) we assume that all Ps which diffuses back to the surface escapes. The parameter E_o is related to the o-Ps diffusion length[8,25] by $L_o=AE_o^n$, where A is the constant in the relation adopted for the mean positron penetration depth:

$$\bar{x}=AE^n . \tag{4}$$

The functional form found for $d_o(E)$ furthermore depends on the assumption that the positron implantation profile is exponential.[27] This latter assumption is open to some criticism.[26,28] With a different implantation profile the functional form of $d_o(E)$ will be different and the parameters (E_o and n) extracted from a fit to experiments will change. Also, the physical quantities (e.g., $D_{\rm Ps}$ and L_o) derived from the fitting parameters may be affected.[26,29] However, their temperature dependences are not much affected.[29] The relation, Eq. (4), between mean penetration depth and incident energy seems to be a good approximation for both electrons[30–33] and positrons,[34] at least for incident energies in excess of approximately 300 eV. Using electron penetration data[29–32] for low atomic number insulators, we expect values of $n=1.75$ and $A=320\pm 100$ Å keV^{-n}. This agrees well with the data of Mills and Wilson[34] for positrons on Al and Cu which give $A=335$ Å keV^{-n} when calculated for ice densities. For energies below about 300 eV, Eq. (4) with the estimated values of A and n probably underestimates the mean penetration depth, at least in insulators.[32,33]

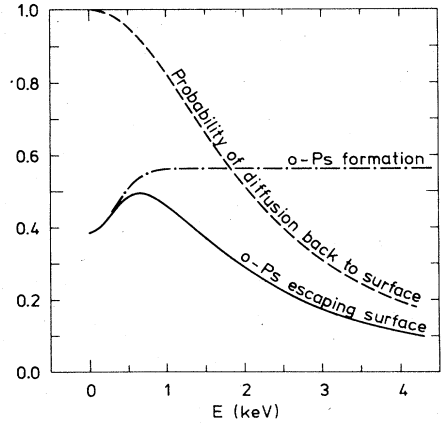

FIG. 4. Sketch of the two factors that determine the shape of the curves in Fig. 3 as described by Eq. (2). The curves are drawn with realistic parameter values for ice. The curve labeled o-Ps formation is the function $p(E)$ given by Eq. (3), the curve labeled as the probability of diffusion back to surface is the function $d_o(E)$ in Eq. (2), and the curve labeled o-Ps escaping surface is $f=p(E)d_o(E)$, Eq. (2).

With these reservations about the model in mind we fitted Eq. (2) to the measured high-energy curves for crystalline ice, at first leaving the parameters p_0, $p_{\max}$, E_1, β, E_o and n as free-fitting parameters. Because of the correlation between these parameters, they showed rather large scatter [e.g., $\bar{p}_{\max}=0.55$, $\sigma(p_{\max})=0.05$; $E_o=1792$, $\sigma(E_o)=129$; $\bar{n}=1.93$, $\sigma(n)=0.13$; $E_1=409$, $\sigma(E_1)=33$; corr$(E_o,p_{\max})=-0.98$; corr$(E_o,n)=0.84$; corr$(E_o,E_1)=-0.79$, where the bar, σ, and corr represents a typical mean value, standard deviation, and correlation coefficient, respectively, of the fitted parameters as determined from several scans at each temperature]. In bulk ice the o-Ps yield is close to 56%,[12] and we subsequently analyzed the data with $p_{\max}$ fixed at 0.56 to reduce the correlation in the fitted values. [The correlation coefficients were now: corr$(E_o,n)=0.43$, corr$(E_o,E_1)=-0.57$, corr$(E_0,\beta)=-0.36$. These values show that the functions $p(E)$ and $d_o(E)$ in Eq. (2) are fairly well separated in the fitting procedure.]

IV. RESULTS AND DISCUSSION

A. Crystalline ice

1. Low energies

A main challenge in the discussion of the results presented in Fig. 2 is to interpret the large variations with incident positron energy of the vacuum o-Ps fraction. For a comparison with the Ore model let us first formulate this model for a solid.[15,35] The lower, well-defined, limit of the Ore gap is given by

$$E_L=I-6.8\text{ eV}-Q_{\rm Ps} , \tag{5}$$

and the upper, probably less sharp, limit by

$$E_U=E^*-Q_+ , \tag{6}$$

where I is the ionization energy, E^* the lowest excitation energy, Q_+ the positron and $Q_{\rm Ps}$ the Ps affinity (equal to the work function) to the solid. E_L and E_U refer to the positron energy in vacuum.

The lowest ionization energy according to the review of ice energy-band structures by Rosenberg *et al.*[36] is 9.8 eV (probably with an uncertainty of about 1 eV). Q_{Ps} is estimated to be -2 ± 1 eV (see Sec. IV A 4). Hence we find $E_L=5$ eV with an estimated uncertainty of ±1.5 eV. This value is in agreement with the incident positron energy at which the steep rise in Ps fraction is observed [Fig. 2(b)], which suggests that an Ore-type process may be responsible for the Ps peak at about 6 eV. We have therefore carried out a Monte Carlo simulation[37] of the positron slowing down and Ps formation in ice considering only the Ore model, and taking into account all four electronic energy bands of importance (with $I=9.8$–10.5 eV, 11.5–12.5 eV, 16.3–16.6 eV, and 27.5–34.0 eV following Ref. 36). This is described in Appendix A. A similar and independent Monte Carlo calculation, which, however, only takes the first band into account, has also been made by Van House *et al.*[38]

The effect of the lower-lying bands having a higher I will be to provide additional channels for Ps formation in competition with positron slowing down by inelastic scattering through excitation and ionization. An additional positron slowing-down mechanism is the two-step process of the formation of energetic Ps followed by collisions with molecules which split up the Ps into an electron and a positron. In order to calculate the contributions from these processes to the total Ps yield, it is necessary to know the positron cross sections for slowing down by inelastic scattering (excitation and ionization) and for Ps formation.[37,39] Such cross sections are not directly available for ice, but as discussed in Appendix A one can make some reasonable estimates. The results of the calculation are shown in Fig. 5. Although the result for curve *d* of Fig. 5 is not identical to the curve for *f* in Fig. 2, there is a striking similarity. With the rather larger uncertainties on some of the input parameters to the calculation, no detailed agreement can be expected, although such an agreement could certainly be obtained by adjusting these parameters. This fact suggests that similar measurements may be used to obtain information on, e.g., cross sections for various positron scattering processes, including Ps formation.

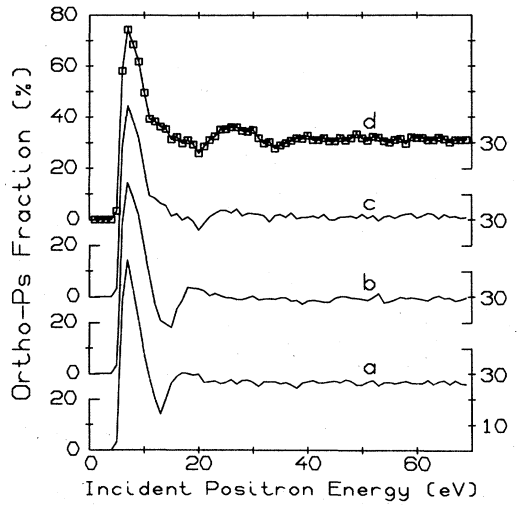

FIG. 5. Calculated fractions of positrons forming *o*-Ps as a function of incident positron energy. The curves were obtained by the Monte Carlo calculation described in Appendix A. The contributions to the total curve, *d*, from the various electronic bands are illustrated by the three other curves. They are results if only one band (curve *a*) (ionization energy $I_1=9.8$ eV), two bands (curve *b*) (I_1 and $I_2=11.5$ eV), and three bands (curve *c*), (I_1, I_2, and $I_3=16.3$ eV) are included in the calculation. In curve *d* the fourth band ($I_4\simeq30$ eV) is also included.

Here we use the results of the Monte Carlo calculation to interpret the various features of *f* in Fig. 2. Below about 5 eV, Ps formation is energetically impossible. The intense peak at about 6 eV is due to Ps formation in the lowest-lying Ore gap. Positron slowing down by phonons will compete with Ps formation and is the likely reason that *f* does not quite reach 75% as it does in the calculations (which do not include phonon scattering). Ore gaps associated with the energy bands around 12 and 16.5 eV contribute to the Ps yield at slightly higher energies than the main peak, thus making the peak asymmetrical. The maximum at around 25 eV arises mainly from Ps formation in the Ore gap associated with the band at around 30 eV. The minimum at about 35 eV (which is most clearly seen in Fig. 2(c), where the scatter of the points is smallest) is due to formation just above this latter Ore gap of Ps which splits up again, leaving the positron at such low energy (<5 eV) that it cannot form Ps a second time. The minimum at about 15 eV (Fig. 2) is probably of the same origin, but associated with the lower-lying Ore gaps (compare curves *b* and *c* of Fig. 5). Positrons with initial energies above about 40 eV will suffer a sufficient number of energy losses to lose memory of their initial energy before Ps formation takes place, resulting in the plateau at these energies.

An important question is whether the relatively large Ps yield at low E (Fig. 2) ascribed to Ore processes can be regarded as representative of bulk ice, or whether the surface strongly influences the Ps yield. The agreement with the Ore model using ionization potentials for bulk ice strongly suggests that the observed Ps formation is a bulk process. However, Ps is able to escape through the surface within a short time, thus preventing possible Ps reactions just after formation. One such reaction could be oxidation of Ps by the positive ion which is created when the positron picks off an electron to form Ps.[40–42] This oxidation process is simply the reverse of the Ps formation process. If Ps is formed far from the surface and with low energy (e.g., by a positron just above E_L), it may be thermalized rather close to the positive ion and hence have a large probability of being ionized (since the electron binding energy to the positive ion is larger than to the positron). Unless the positron regains all its kinetic energy in this reverse process and hence is able to form Ps again, the described process tends to reduce the Ps yield compared to the situation where Ps has a high probability of escaping through the surface. In order to estimate quantitatively the importance of the Ps oxidation, it is necessary to know, e.g., the Ps slowing-down cross sections. At present they are not available. However, it seems unlikely that Ore contributions to the total Ps yield

will be reduced to an insignificant level in bulk ice.

Still, it should be emphasized that an appreciable fraction of the total Ps yield in bulk ice must be a result of spur processes. First of all one would expect this, since the spur model of Ps formation[18,19] has been successful in explaining and predicting a number of experimental findings in liquids and has also been able to account for observations of Ps yields in high-density gasses.[42] Secondly, in our results the rise of f for $E \gtrsim 100$ eV (Fig. 3) is interpreted to be a result of spur processes[21,38] (see also Sec. IV A 3).

Furthermore, we should mention that in the present paper we have used the terminology that Ps formed from a positron with energy in an Ore gap was formed by an Ore process. On the other hand, Mogensen has argued[40] that even at Ore-gap energies, the Ps formation process in condensed matter is more complicated than just being the one-step reaction usually assumed for an Ore process. He therefore argues that the formation should rather be considered to be a spur process in a single-electron spur.

2. *Electron flooding*

The flood gun (see Sec. II) was used several times to neutralize the sample charging, which manifested itself by a higher and somewhat smeared-out beam onset threshold. After flooding the onset voltage was again sharp. Furthermore, the structure in the curve of f versus positron energy (Fig. 2) had completely disappeared, f being constant equal to about 37% for $0 < E < 65$ eV, i.e., the same level as in Fig. 2 for the highest energies. The structure of Fig. 2 gradually reappeared with time after the flooding, being fully recovered after about 10 hours at 147 K. Although one or two rather speculative explanations for these observations can be proposed we have at present no convincing interpretation of the curious effect of electron flooding. More detailed investigations are required. We observe no effect of flooding with electrons on the high-energy curves (~ 50 eV $< E < 4.5$ keV, Fig. 3).

3. *High energies*

Figure 3 illustrates that a major effect of temperature on the high-energy curves is a decrease of the maximum value of f with decreasing temperature. At the highest energies the curves coincide. This part of the curves is determined by the back-diffusion of o-Ps [$d_o(E)$ in Eq. (2)]. Hence we see directly that Ps diffusion is largely temperature independent. This is also reflected in the E_o values obtained by fitting Eq. (2) to the curves, as seen in Fig. 6. The E_o values for the two samples deviate by about 12% (maybe due to some trapping of Ps in defects in the second sample), but both of them are essentially temperature independent below 100 K and show only a small increase at higher temperatures. The average E_o values for the two samples result in Ps diffusion coefficients D_{Ps} of 0.11, and 0.30 cm^2/sec.

The values of D_{Ps} compare favorably with other estimates. HF doping of ice[35] creates defects, probably vacancies, which trap Ps. From the HF-concentration dependence of the trapped Ps fraction one may deduce a lower limit of the diffusion coefficient, assuming that the trapping is diffusion limited and that each HF molecule gives rise to one trap. This lower limit is $D_{Ps} \simeq 10^{-2}$ cm^2/sec. The fact that the present results are at least an order of magnitude larger suggests that either the trapping rate into vacancies is not diffusion limited (which is reasonable since of the order of 1 eV has to be dissipated to phonons in the trapping process) or that the vacancy concentration is only about one-tenth of the HF concentration.

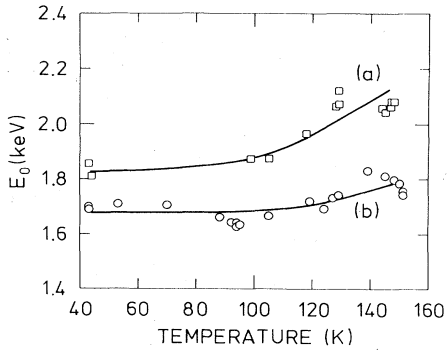

FIG. 6. Values of E_o, derived by fitting Eq. (2) to spectra like those in Fig. 3, as a function of temperature. Data for two different crystalline samples are shown: (a) crystal 1, (b) crystal 2.

Using Dupasquier's approach[15] to calculate the Ps diffusion constant from the width of the narrow p-Ps component in angular correlation curves, we can estimate D_{Ps} from the high resolution data for ice in Ref. 43. Depending upon the assumptions made about the model, we obtain a temperature independent $D_{Ps} \sim 0.07$–0.3 cm^2/sec, in good agreement with the present more direct measurements.

Measurements of electron mobilities in irradiated[44] ice give values of 20 ± 10 cm^2/V sec at 150 K. By the Nernst-Einstein equation this is equivalent to a diffusion coefficient of about 0.2 cm^2/sec. Since the electron and Ps have a main interaction with the lattice in common, viz. the exchange interaction, one would expect their diffusion coefficients to be roughly the same, as seems to be the case, although probably the diffusion coefficient for Ps is somewhat larger, because Ps is neutral. This difference is not brought out by the present comparison, but requires more detailed investigations for both electrons and Ps.

The rise in f between 50 eV and roughly 700 eV (Fig. 3) we ascribe to an increase in the total Ps yield with positron incident energy as we shall discuss in the following. Figure 2(b) shows that the o-Ps fraction leaving the surface may be as high as about 66% (or higher) for Ps formed in the Ore gap. This is a major fraction of the highest possible value of 75% (Fig. 5). Hence, we conclude that most (if not all) of the Ps formed in the Ore gaps at low energies escapes the surface. For E values of about 50 eV the o-Ps fraction leaving the surface is 40% or lower (Figs. 2 and 3). Hence, the total o-Ps yield at these energies is less than $40\% \times \frac{75}{66} = 45\%$. On the other hand, studies of bulk ice[12] show that for high positron energies the o-Ps yield is about 56%. Therefore the Ps yield must increase with positron energy somewhere in the

range 50 eV to several keV.

As argued above (Sec. IV A 1), the constant f in the (50—100)-eV range is attributed mainly to Ps formation in the Ore gaps at lower energies. Hence, if only Ore processes were responsible for the Ps formation the total Ps yield should be independent of the initial positron energy for $E \gtrsim 50$ eV, and no increase in f should be observed. We therefore ascribe the observed rise in f to a recombination of thermalized positrons with thermalized excess electrons created during positron slowing down, i.e., a result of spur processes. This is further discussed in the following.

A reasonable assumption is that the slowing-down properties of the positron in ice are almost the same as for the electron in water (except maybe at energies of a few eV). Hence the positron creates on average an ion pair for about every 25 eV of energy loss for E above ~ 100 eV.[45] (Below ~ 100 eV more than 25 eV is required on average.[45]). Furthermore, the stopping power for positrons in ice in the energy range from 50 to 1000 eV is 2 ± 1 eV/Å.[45] Hence, during the positron slowing down in this energy interval the distances between the creation of ion pairs are on average much smaller (~ 10 Å) than the thermalization distance for the electrons[30] (~ 300 Å). The simplified picture which emerges is then the following. A positron of a certain initial energy in this range (which has not formed stable Ps by the Ore process) slows down with the creation of a number of positive ions and of the same number of electrons which after thermalization are distributed over a region of a size of roughly 300 Å. In addition, a number of radicals and excited molecules are created.[18,19] This configuration may also be referred to as overlapping spurs. On the above assumptions the positron will slow down somewhere inside the region of the electron distribution. Since essentially all the electrons will be separated from the positron and the positive ions by less than Onsager's critical radius for escape,[18] the electrons will be attracted by the positive charges and a recombination will take place. If one of the electrons recombine with the positron, Ps is formed. At low energies (50—100 eV) where only a few electrons (of which more than one is lost through the surface[46]) and positive ions are present the probability of Ps formation is low, while at higher energies where many positive ions and excess electrons are created there is a higher probability that one of the electrons recombines with the positron. Thus, we can understand the increase of the Ps yield with increasing incident positron energy for $E > 50$ eV. This increase was also reproduced in the Monte Carlo calculations of Van House *et al.*[38] With increasing energy also the mean positron penetration depth increases (with a large scatter of the positron trajectory end point, ~ 300 Å, both perpendicular and parallel to the surface; see, e.g., Ref. 28). When this depth is about the size of the excess-electron slowing-down range (~ 300 Å) the positron can roughly speaking no longer recombine with the electrons created by itself close to the surface, and the Ps yield will become energy independent. This positron penetration depth is equivalent to an incident positron energy of about 1 keV [Eq. (4)], in qualitative agreement with experiments (Fig. 3).

The temperature dependence of the curves in Fig. 3 (which is reversible) is mainly reflected by the decrease of the parameter E_1 [Eq. (3)] with increasing temperature. At low temperatures E_1 is roughly constant (440 ± 45 eV) up to approximately 100 K, and then decreases to 330 ± 30 eV at 150 K. This is ascribed mainly to a temperature dependence of the slowing-down range of the excess electrons.[21] This range is expected to decrease at higher temperatures as a result of a shorter mean free path for inelastic collisions with phonons.[21] Hence, the slowing-down range of roughly 300 Å mentioned above is expected to be smaller at higher temperatures. This in turn decreases the positron mean penetration depth at which the Ps yield becomes energy independent ($f = p_{\max}$). Hence also E_1, the energy at which the Ps yield $p(E_1) = p_0 + 0.39(p_{\max} - p_0)$ [Eq. (3)], decreases.

In the above discussion we argued that at least in the low-E range most ($\gtrsim 85\%$) of the Ps formed would escape the surface. Also, in the interpretation of the high-energy curves (Fig. 3) we have assumed (Sec. III) that all Ps diffusing back to the surface escapes. This does not seem to be an unreasonable assumption, since a Ps atom being ejected from the surface with a kinetic energy of 2 eV (see below) will traverse a possible surface trap of, e.g., 10 Å width in less than 2×10^{-15} sec. This time is about the same as for a positron being emitted from a metal surface. In that case the positron may lose enough energy by electron-hole pair creation to become trapped in a surface state. This low-energy-loss process is not available in an insulator. It is therefore likely that Ps will escape the surface. However, it is worthwhile briefly to consider the possibility that the neutral Ps atom might lose enough energy in this short time to become localized in a "surface state" (similar to physisorption).

If all Ps becomes weakly bound to the surface at low temperatures, having a very small overlap with the ice (to account for the high fraction of 3γ decays), but desorbed thermally at 150 K, this could roughly explain the main features of the temperature effect in Fig. 3. However, the Doppler-broadening results below could not be accounted for. If, on the other hand, only 10—20% of the Ps became surface trapped at low temperatures (the rest escaping) with a relatively large overlap with the ice, but could thermally detrap at 150 K (binding energy $\simeq 0.1$ eV), this could approximately produce the temperature variation in Fig. 3 and be in reasonable agreement with the Doppler-broadening results. In this model $p_{\max}$ [Eq. (3)] becomes slightly temperature dependent. Hence, the fitted parameter values [Eqs. (2) and (3)] will deviate somewhat from the ones determined for a temperature-independent $p_{\max} = 0.56$ (Sec. III).

From the present experimental data we can hardly determine which of the two explanations of the temperature effect in Fig. 3 (if any) is the correct one, although as argued above the latter seems less likely.

4. *Doppler broadening*

The results of the Doppler-broadening measurements given by the S and W parameters are shown for low energies in Fig. 7 and for high energies in Fig. 8. For low en-

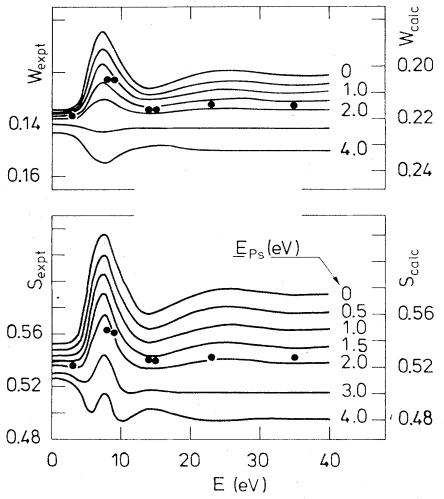

FIG. 7. Doppler-broadening parameters S and W as a function of energy. The solid circles are measurements for crystal 1 at 145 K (left-hand scale). The curves are calculated for different kinetic energies of Ps perpendicular to the surface, E_{Ps}, as described in Appendix B (right-hand scale). The left- and right-hand scales are somewhat shifted relative to each other.

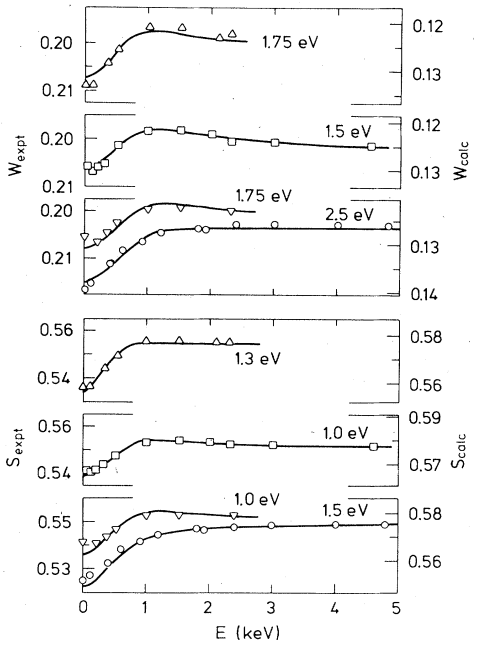

FIG. 8. Measured Doppler-broadening parameters S and W as a function of positron incident energy and for different temperatures: ○,▽ 45 K; □, 95 K; △, 150 K. The circles are for crystal 1, the other symbols for crystal 2 (left-hand scale). The curves are the best-fitting curves calculated as described in Appendix B (right-hand scale). Right- and left-hand scales are somewhat shifted relative to each other. The energy written at each curve is the value of E_{Ps} (kinetic energy of Ps perpendicular to the surface) for the calculated curve.

ergies the characteristic features of the data is a maximum in S (and equivalent minimum in W) at the energies where f shows a maximum (Fig. 2). The high-energy curves, on the other hand, show a gradual increase in S (decrease in W) up to 1—2 keV and a constant value at higher energies, maybe with a weak maximum in S in some cases (and a somewhat more pronounced minimum in W). In order to understand the shapes of these curves we have computer-generated Doppler-broadening curves and calculated the S and W parameters from them. To do so we have used the information from the measurements of f versus energy (of which some are shown in Figs. 2 and 3). From these latter data the fraction of o-Ps, p-Ps, and "free" positrons in the bulk ice and in vacuum as functions of energy can be obtained. The contributions of these various states to the Doppler-broadening spectrum can be obtained from the knowledge of shapes of angular correlation curves in ice.[12] An additional effect to be taken into account is the Doppler shift of annihilation quanta from Ps which is ejected from the sample into the vacuum. The most important influence of this effect on the Doppler-broadening spectrum comes from p-Ps whose narrow annihilation line may be redshifted appreciably, causing an effective widening of the Doppler-broadening curve. The calculations are described in detail in Appendix B. In Fig. 9 we show one set of results of these calculations. The figure shows the calculated S and W parameters as functions of positron incident energy for different values of the energy E_{Ps} with which Ps leaves the sample surface. The Ps velocity is assumed perpendicular to the sample surface and thus away from the detector, giving rise to a "red shift" of the p-Ps annihilation line. The equivalent curves for the other sam-

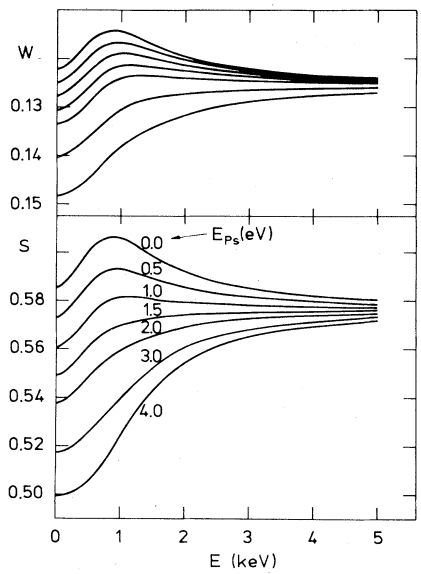

FIG. 9. Calculated Doppler-broadening parameters S and W as a function of positron incident energy for crystal 1 at 45 K (Appendix B). E_{Ps} is the Ps kinetic energy in vacuum perpendicular to the surface. The E_{Ps} values are the same for the S and W curves. The differences between curves with different E_{Ps} values are due to red shifts of the 511-keV annihilation line of p-Ps in vacuum.

ple and at other temperatures are very similar to those in Fig. 9.

The calculated curves were compared to the experimental points. By shifting the absolute values slightly for the S and somewhat more for the W parameters, good agreement can be obtained between experimental results and calculations for E_{Ps} values of 1.0—1.5 eV for S and 1.5—2.5 for W as shown in Fig. 8. The difference in absolute values between calculations and experiments may be associated with an additional background which has not been accounted for in the calculations.[24] Such a background will give rise to a decrease in S and an increase in W which is the trend indicated by the data. Furthermore, some simplifying assumptions have been made, e.g., the shapes of the angular correlation curves for positrons at the surface and in the bulk are assumed the same. This assumption is most serious for the low-energy curves (Fig. 7). Since S will be less affected than W by these problems (and especially for higher energies), we attach more significance to the E_{Ps} values from the S parameter fitting in Fig. 8.

The results show that Ps is ejected from the ice surface with a kinetic energy of a few eV (see further below). This energy may arise from two sources. One would be that Ps formed in the bulk crystal has not been thermalized before it escapes the surface. Ps formed closed to the surface, i.e., for small E, may on average have higher energy when escaping than Ps formed at larger depths. A typical thermalization distance is probably about the same or somewhat larger than that of the electron,[15] i.e., corresponding to the mean implantation depth at $E \sim 1$ keV. However, since the curves for constant E_{Ps} (independent of E) are in good agreement with the shapes of the measured curves (Fig. 8), we have evidence that only a minor fraction of E_{Ps} is due to nonthermalization.

The other possible source of a nonzero E_{Ps} is a negative Ps affinity, Q_{Ps} [Eq. (5)], to the crystal.[47] A repulsive exchange interaction exists between the Ps electron and the surrounding molecules. This is manifested in molecular solids by Ps trapping in vacancies and clusters of vacancies and in molecular liquids by the existence of Ps bubbles.[13] Hence, we would expect thermalized Ps that has diffused to the surface to be expelled into the vacuum with a kinetic energy close to $-Q_{Ps}$. [Inelastic processes at the surface may reduce the kinetic energy somewhat below $-Q_{Ps}$ (see discussion in the preceding section).] This kinetic energy will not depend on the depth of Ps formation, in apparent agreement with experiments (Fig. 8). Hence, we take this agreement as evidence that the main part of the kinetic energy of the Ps leaving the surface is due to the negative Ps affinity to the crystal, and only a smaller fraction is a result of nonthermalization.

An important assumption in the calculations (Appendix B) was that the Ps velocity is perpendicular to the ice surface, i.e., directly away from the detector. For some metals it has been shown that essentially thermalized positrons are ejected due to their negative work function mainly perpendicular to the surface.[48] It seems reasonable to expect the same for Ps emission from a molecular crystal surface, since the gradient of the potential (which gives rise to the ejection) is on average perpendicular to the surface. Possible inelastic processes at the surface may though perturb the perpendicular emission to some extent. This problem should be further investigated by, e.g., angle-resolved Ps emission measurements. The present samples are probably polycrystalline with the crystallite surfaces oriented at an angle to the average planar surface. Hence, even if Ps is ejected perpendicular to the surface locally with the velocity v_{Ps}, it may not be directly away from the detector. Since only the velocity component $v_\perp$ pointing away from the detector contributes (in first order) to the Doppler shift, the shift will be reduced compared to that calculated from v_{Ps} (Appendix B). If the reasonable approximation is made that Ps is ejected uniformly within a 90° cone (the angle between the average surface normal and maximum deviation from it is 45°), we obtain $\langle v_\perp \rangle = 0.85 v_{Ps}$, equivalent to a total kinetic energy of the ejected Ps being about 38% larger than the values obtained in the fitting of Figs. 7 and 8.

Hence, we obtain values of Q_{Ps} in the two cases of $-(1.0—1.5)$ and $-(1.4—2.1)$ eV. Since some minor contribution to E_{Ps} probably arises from nonthermalization an inelastic surface processes as discussed above, we finish this discussion of the Doppler-broadening data by concluding that a conservative estimate of the Ps affinity to ice, Q_{Ps}, is -2 ± 1 eV. A direct measurement of the maximum energy of emission of Ps from a MgO surface (0.8 ± 0.2 eV) has previously been reported.[49] It would be very interesting also to measure the Ps velocity distribution for ice directly.[50]

5. *Positron scattering*

When the positrons enter the target chamber they pass through an accelerator grid.[9,11] In most of our experiments this grid was at a potential about 1 V below the moderator voltage (e.g., + 24 and + 25 V, respectively). Hence, if the incoming positrons are scattered off the sample with 1 eV or more loss of energy parallel to the beam direction (e.g., an elastic scattering at an angle) they do not have enough energy to pass the accelerator grid and will be repelled back into the sample. As a result all positrons will annihilate at or close to the sample, and the total count rate in the detector will be independent of E, an illustrated in Fig. 2(a). Some measurements were carried out with the accelerator grid grounded. This allows positrons backscattered from the sample to escape the target region, being guided by the magnetic field, and to annihilate far from the detector. This will reduce the total count rate as illustrated in Fig. 10, curve *b*, which also shows the result for a + 24 V grid bias (curve *a*). At the highest energies both curves are flat, suggesting that only little backscattering takes place.

Hence, they were normalized at 100 at these energies and the difference calculated (Fig. 10, curve *c*). This measurement is analogous to those reported by Mills and Platzman[51] for Al and Cu. It is important to note that the Ps fraction versus E was identical for cases *a* and *b*. Hence, the difference in Fig. 10 is not related to Ps formation. Furthermore, it shows that the backscattered positrons which are directed back again into the sample by the accelerator grid enter the sample with essentially the same

energy as the first time. Thus, the first scattering has been essentially elastic.

This suggests that we have observed low-energy-positron diffraction (LEPD) from the ice surface (maybe with some of the structure due to positron surface-resonance scattering[52]). In Ref. 53 we showed a curve resulting from a simple calculation of the energy dependence of the Bragg diffraction intensity for polycrystalline ice Ic, based on LEED data. The calculated curve has some similarity to the measured scattered intensity (Fig. 10, curve *c*). However, such a simple calculation cannot be expected to give very detailed agreement.[54] To further study the observed phenomenon, proper LEPD calculations should be compared with measurements on oriented single crystals done with good energy and angular resolution.[54] That we do observe a diffraction phenomenon is supported by the fact that for amorphous ice no structure like the one in Fig. 10 was observed.

It should also be added that after electron flooding of the crystal the structure in Fig. 10, curve *b*, disappears and the curve becomes identical to the curve *a*. Maybe this is a result of the potential fluctuations introduced in the surface by the electrons.

6. *Sputtering*

In order to study the effect of near-surface damage, we bombarded crystalline ice at 44 K with 3-keV Ne^+ ions to a dose which sputters away about 2000 Å of the surface[55] and leaves a distribution of damage into the crystal with a mean depth of 50—100 Å, and with a tail stretching to a few hundred Å depth.[56] Measurements of f were made on the sample as-sputtered and while it was allowed to slowly warm up. Also, Doppler-broadening curves were recorded at the lowest and highest temperatures. The results are shown in Fig. 11. Clearly there is a very strong effect of the ion bombardment on f.

From earlier studies[12,43,57] it is known that radiation damage in ice affects Ps in mainly two ways, i.e., firstly Ps formation is partly inhibited, and secondly the Ps which is formed may become trapped in vacancies and vacancy clusters. Hence, we should expect the Ne^+ bombardment to give rise to a decrease of the spur contribution to the Ps yield in the damaged region, i.e., a slower rise of $p(E)$ (curve labeled *o*-Ps formation in Fig. 4) due to the inhibition. Furthermore, we should expect that trapping of Ps in defects in the damaged region should reduce $d_o(E)$ (curve labeled probability of diffusion back to surface in Fig. 4) compared to the curve in Fig. 4. A rough quantitative account of these two effects can be made by putting $E_1 \simeq 1000$ eV and multiplying d_o with $0.5+0.5\exp(-E/600\text{ eV})$ in Eq. (2). The resulting $f(E)$ curve is in very good agreement with the as-sputtered curve [open circles, Fig. 11(a)], on the assumption that only 70% of the Ps reaching the surface escapes (one would expect that even if Ps reaches the surface there will be a competition between escape and trapping into defects). The fact that sputtering damage gives rise to a curve which can be accounted for in the above way provides strong support to the interpretation given earlier (and sketched in Fig. 4) of the curves in Fig. 3.

During warm-up of the sputtered ice a change of the $f(E)$ curve is observed for temperatures above approximately 100 K. This is in agreement with the earlier find-

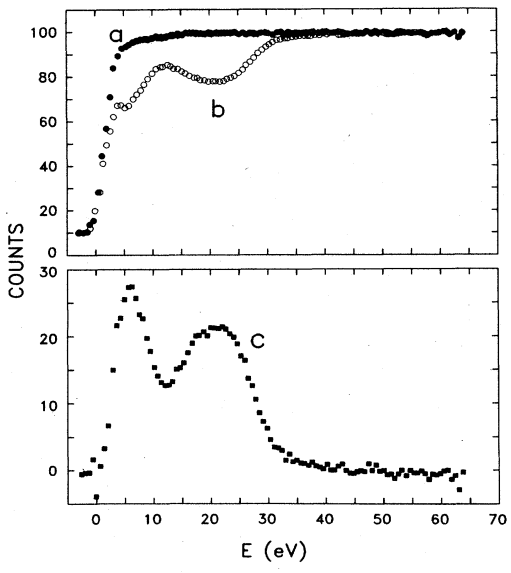

FIG. 10. Evidence for positron backscattering. Curve *a* shows total countrate versus E for an accelerator-grid voltage (V_a) of 24 V. Curve *b* is like curve *a*, but with $V_a=0$ V. Curves *a* and *b* are normalized to 100 at the highest voltages. Curve *c* is the difference between curves *a* and *b*. The beam onset is not as sharp in curve *a* as in Fig. 2 due to a few volts charging of the sample.

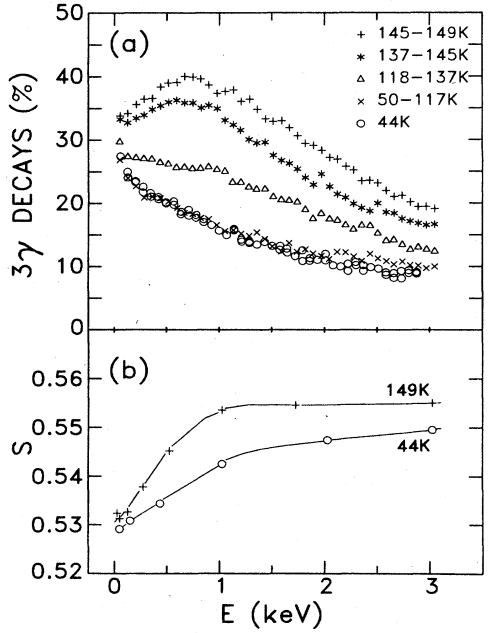

FIG. 11. Effect of sputtering and subsequent annealing of crystalline ice as reflected (a) in the fraction of 3γ decays, f, and (b) in the Doppler-broadening peak parameter, S. In (a) the points were obtained as a function of increasing energy, while the sample was warming up through the indicated temperature intervals. The curves in (b) are drawn to guide the eye.

ing that at 100 K and above vacancies are migrating and the radicals responsible for Ps inhibition disappear.[57] At the highest temperatures the curves show the shape characteristic for crystalline ice. However, it should be noted that the (145—149)-K curve at the highest energies shows a higher 3γ rate than observed both for other samples (Fig. 3) and for the same sample before sputtering, while at the lower energies ($E \lesssim 1$ keV) it is opposite. Thus the enhancement at higher E is not a result of an enhanced probability of Ps emission through the surface due to, e.g., sputter cleaning of the surface. Neither is it obvious why sputtering and subsequent annealing should give rise to a larger diffusion coefficient for Ps. An explanation might be that the treatment gives rise to a very irregular surface. It is known that large cavities may be formed in ice which has been irradiated at low temperatures and subsequently heated.[57] If a high density of cavities coalesce very large cavities or even a very irregular surface may result. With such a surface structure Ps would on average have a shorter diffusion distance to a free surface than for a sample with a planar surface.

The Doppler-broadening S parameter [Fig. 11(b)] also clearly reflects the difference between the as-sputtered (44 K) and the annealed (149 K) ice, the slow rise of the 44-K curve being the combined effect of the Ps inhibition and trapping. At 3 keV the two curves differ mainly because of the difference in the fraction of 3γ decays.

B. Amorphous ice

The results for as-grown amorphous ice are shown in Fig. 12. They are significantly different from those for crystalline ice (Fig. 2 and 3). At low energies f is constant, independent of positron energy from $E=0$ eV to at least 70 eV. This behavior is identical to that for e^--flooded crystalline ice (Sec. IV A 2), except that f is slightly lower for the amorphous ice. The beam onset is at a nominal positron incident energy $E=-3.5$ eV, i.e., 2.6 eV lower than for crystalline ice. This difference cannot be accounted for by contact potential differences, but may be due to negative charging of the sample. The charging probably occured by electrons from the ionization pressure gauge which were trapped in the amorphous structure during the growth of the sample. Such electrons will probably have a binding energy of only 1—2 eV, and even zero incident energy positrons can form Ps with them. Thus, the low-energy results may have the same origin as the results for e^--flooded crystalline ice, and hence be an effect resulting from the presence of excess electrons and not necessarily from the amorphous structure in itself. To resolve this question more investigations are needed.

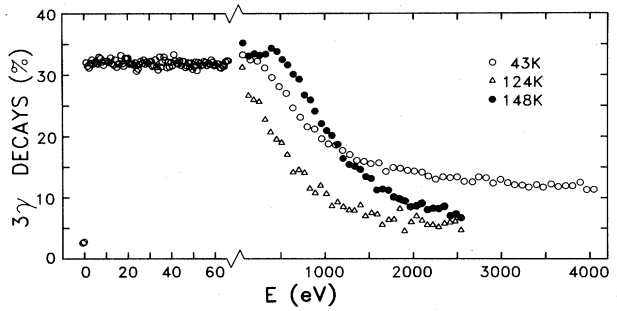

FIG. 12. Amorphous ice. The fraction of 3γ decays, f, as a function of positron incident energy. At 43 K, f was measured both in the low- and the high-energy regions. The beam onset was found at a nominal positron energy of -3.5 eV. At higher temperatures only the high-energy region was measured. Major changes in the curve shapes occurred at about 100 and 135 K. The three types of curves are associated with amorphous ice containing large cavities (43 K), amorphous ice without these cavities (124 K), and crystalline ice with defects (148 K).

For higher energies f decreases much more rapidly than for crystalline ice (Fig. 3), but levels off at the highest energies. As mentioned in Ref. 21, we interpret the rapid decrease as due to a much shorter Ps diffusion length (equivalent to a diffusion coefficient $D_{Ps} \sim 10^{-3}$ cm^2/sec) in amorphous ice where Ps may become trapped in the cavities in the structure. The leveling off at high energies shows that positrons injected a few thousand angströms into the sample may annihilate by 3γ decay. The most likely explanation of this is that the as-grown amorphous ice contains large cavities in which Ps may become trapped. In these cavities the o-Ps pick-off rate will be sufficiently low to allow for an appreciable fraction of the o-Ps atoms to decay by intrinsic 3γ annihilation. One can estimate[21] that the cavities must have average diameters of ~ 17 Å or larger. Cavities of this size are not unrealistic, since similar sized and larger voids have been observed in amorphous semiconductors.[58,59] Furthermore, it was recently suggested[60] that preparation of amorphous ice in a way similar to ours may lead to a highly porous solid with a network of pores or voids [while putting a baffle between the vapor inlet tube and the cold plate (Fig. 1) would lead to a nonporous solid]. Somewhat smaller voids have also been observed in crystalline ice after irradiation or HF doping and subsequent annealing.[12,57]

An extreme case of a "highly porous solid" would be one with a very irregular surface (where pores from the surface penetrates deep into the solid). Such a structure may also give rise to the observed high level of 3γ decays at high E (Fig. 12) as briefly discussed in the preceding section.

On annealing the amorphous ice, the curve $f(E)$ changes at about 100 K from the one shown with open circles to the one shown with triangles in Fig. 12. No changes occur until 135 K above which temperature the curve shown with solid circles is measured. This curve is unchanged at higher temperatures until the ice disappears due to sublimation. We interpret the transition at 100 K as being the result of the disappearance and/or coalescence of the cavities, the sample remaining in the amorphous phase. This annealing effect is consistent with observations of annealing of voids in amorphous Ge (Ref. 58) and with suggestions put forward about the defect structure in both amorphous ice[60] and semiconductors.[61] Finally, the amorphous sample crystallizes at 135 K, a crystallization temperature found also in other studies of amorphous ice.[14] The curve is now consistent with the results for crystalline ice (Figs. 3 and 4) if a small E_o value (≈ 600 eV) is assumed. A low value may result from Ps

trapping in defects left over after the phase transition. It would be very interesting to study amorphous ice in more detail also by conventional positron annihilation techniques.

V. SUMMARY AND CONCLUSIONS

The present work constitutes a study of crystalline, amorphous and irradiated ice using monoenergetic positrons of energies 0—4.5 keV. These positrons were injected into the ice and measurements were carried out of the fraction of 3γ annihilations (essentially equal to the fraction of o-Ps escaping the ice surface into the vacuum) and of the Doppler broadening of the 511-keV annihilation γ-energy line.

Important information has been obtained about the Ps formation probability as a function of positron energy in crystalline ice. At low energies (0—65 eV) the Ps yield shows large variations (Fig. 2). This was explained as Ps formation in the so-called Ore gaps, a conclusion strongly supported by an Ore-model Monte Carlo calculation of the positron slowing down and Ps formation processes (Fig. 5). At higher energies ($E > 100$ eV) the Ps yield increases with energy as a result of thermalized electron-positron recombination, i.e., spur processes (Fig. 3). The possible influence of the surface on the balance between the Ore and the spur contributions to the total Ps yield was briefly discussed.

Ps diffusion to the surface was observed for positron energies above 700 eV (Fig. 3). The Ps diffusion coefficient was $D_{Ps}=0.17\pm0.09$ cm^2/sec with only a weak temperature dependence (Fig. 6).

Doppler broadening data were compared with calculations based on the 3γ yields (Figs. 7—9). From this the Ps affinity (or work function) to the ice was estimated at -2 ± 1 eV.

Evidence for elastic scattering of positrons from the surface of the crystalline ice in the low-energy region was obtained. It was argued that the observation was probably due to low-energy-positron diffraction (LEPD). The intensities of scattered positrons were as high as 28% (Fig. 10). No scattering peaks were observed in the amorphous ice.

Ion sputtering of crystalline ice at 44 K resulted in a strong reduction of the 3γ yield (Fig. 11), in agreement with the expected effect of the sputtering damage, i.e., inhibition of Ps formation and trapping in defects of Ps. On heating above 100 K (the vacancy migration temperature) the curve characteristic of crystalline ice was gradually recovered.

In the amorphous ice the 3γ yield was energy independent at low positron energies (Fig. 12). This lack of a structure, similar to that found in the e^--flooded crystalline ice, was thought to be associated with electron trapping in the amorphous structure during sample preparation. A rapid decrease of the 3γ yield at higher energies was interpreted as a result of Ps back-diffusion to the surface with a diffusion coefficient of $D_{Ps}\sim10^{-3}$ cm^2/sec, i.e., more than 2 orders of magnitude smaller than in crystalline ice. The data also showed evidence for the presence of large cavities (>17 Å diam) in the as-grown amorphous ice. These voids disappeared after annealing to about 100 K.

Being the first (to our knowledge) slow-positron study of a molecular crystal, the present work of course leaves a number of questions and problems. First of all it would be very interesting to study other molecular crystals with low-energy positrons, in order to firmly establish the relationship between electronic structure and Ps yield, and to determine the Ps diffusion coefficient. Higher precision can be obtained by using positrons of higher energies than the 4.5-keV maximum of this study. In this connection it might be interesting to look at crystals with no bulk Ps formation (e.g., anthracene) to obtain additional information about the influence of the surface on the Ps formation. The curious effect of flooding the ice surface with electrons should be studied in a more detailed and quantitative way than has been possible in the present work. The electronic structure of amorphous ice is very similar to that of cubic ice. Hence, following the interpretation of the present data we should expect a structure similar to that of Fig. 2 for uncharged amorphous ice. It would be an important test of our interpretation to perform this experiment. The voids discovered in the as-grown amorphous ice would be better studied by conventional positron lifetime measurements. Such an investigation would add important information about the structure of amorphous ice and would be valuable for comparison with similar voids in amorphous semiconductors. Finally, a direct measurement of the kinetic energy and angular distribution of Ps ejected from an ice surface would be very interesting.

ACKNOWLEDGMENTS

Discussions with F. M. Jacobsen and O. E. Mogensen about the present data have been of great value. Also, we want to thank J. Schou, M. Charlton, R. Nieminen, and I. K. MacKenzie for discussions; F. M. Jacobsen for permission to use his Monte Carlo program; and N. J. Pedersen for technical assistance. This work was supported in part by the Division of Materials Services, U.S. Department of Energy, under Contract No. DE-AC02-76CH00016.

APPENDIX A: MONTE CARLO CALCULATION OF THE PS YIELD

In this appendix we discuss a Monte Carlo calculation of the slowing down of the positrons and of the Ps formation as a function of the positron incident energy in the low-energy region ($0<E<70$ eV). We use a slightly modified version of a Monte Carlo program written by Jacobsen for calculations on gases.[37] The model used in the calculation assumes that a positron may be slowed down by electronic excitations and ionizations and by forming energetic Ps which subsequently splits up in collisions with molecules, leaving the positron with lower energy than before the Ps formation. Stable Ps is considered to be formed when the Ps kinetic energy is less than its binding energy (or a few eV higher, see below), i.e., for positrons with energies in the Ore gap. Slowing down of positrons by, e.g., phonon scattering has been assumed in a first approximation to be a second-order effect com-

pared to the above-mentioned slowing-down processes, and has therefore not been included. Furthermore, we assume that all the slowing-down processes are fast compared to the lifetimes of the positron. These lifetimes therefore do not enter into the calculations. Finally, the Ps formation between a positron of energy below the lowest Ore gap and one of the free electrons which may have been generated during the slowing down (spur model) has not directly (see below) been considered in the calculations.

For the calculation of the slowing down relative, energy-dependent cross sections, σ_j, are ascribed to the various slowing-down processes mentioned above. A random number, $\mathscr{R}_1$, determines via the cross sections which of the slowing-down processes shall be chosen for a positron of a certain energy, E. If

$$\sum_{j=1}^{m}\sigma_j(E)\leq\mathscr{R}_1\sum_{j=1}^{N}\sigma_j(E)<\sum_{j=1}^{m+1}\sigma_j(E)\ , \tag{A1}$$

the process associated with the cross section σ_{m+1} is chosen. N is the total number of possible processes, and $\mathscr{R}_1$ here and below represents a number which is evenly distributed between 0 and 1. For each of the scattering events the positron suffers a certain energy loss (further discussed below), unless stable Ps is formed. The calculation scheme is the following. A positron is given a certain initial energy, $E_{\rm in}$. By Eq. (A1) a scattering process is chosen and the appropriate energy loss, ΔE_1, is subtracted from $E_{\rm in}$, unless stable Ps is formed. Then Eq. (A1) determines a new scattering process at energy $E=E_{\rm in}-\Delta E_1$ and the associated energy loss ΔE_2 is subtracted from the positron energy. This procedure continues until either stable Ps is formed or the positron is slowed down below E_L, the lower limit of the lowest Ore gap, where Ps formation is energetically impossible within the model. This calculation is made for 2000 positrons for each $E_{\rm in}$. The Ps yield is then determined as the fraction of the positrons which form stable Ps. $E_{\rm in}$ is changed in steps of 1 eV over the range $0\leq E_{\rm in}\leq 70$ eV.

Rosenberg *et al.*[36] have compiled some of the available data on the electronic energy-band structure of ice. Their results are three bands of a width of about 1 eV, the lower limits of the ionization energy I_i being 9.8, 11.5, and 16.3 eV, and one band of energy 27.5—34 eV (apart from a band $I_i\sim 540$ eV from oxygen core electrons). The lowest conduction-band energy they estimate at -2.5 eV, while Ref. 62 gives a value of -0.1 eV. Using the mean value, we find the lowest excitation energies, E_i^*, for the four bands at 8.5, 10.2, 15.0, and 26.2 eV.

The positron energy losses associated with the different inelastic scattering processes were estimated as follows. When an excitation event is chosen [Eq. (A1)] the energy loss is taken as the proper excitation energy mentioned above. In an ionization process the positron may lose more than the ionization energy. Based on the data of Turner *et al.*[45] on electron energy deposition in liquid water, we approximate the energy loss by

$$\Delta E_j^I=\begin{cases}(2E/3-I_j)\mathscr{R}_1+I_j & \text{for } E\geq 1.5I_j,\\ I_j & \text{for } 1.5I_j>E\geq I_j.\end{cases} \tag{A2}$$

If Ps is formed by a positron with kinetic energy E^b (b denotes before), the Ps kinetic energy is given by $E_{\rm Ps}=E^b-Q_+-I_i+6.8\ {\rm eV}+Q_{\rm Ps}$, where Q_+ and $Q_{\rm Ps}$ are the positron and Ps work functions (equal to the affinities of the particles to the crystal relative to the vacuum level), and 6.8 eV the vacuum binding energy of ground state Ps.

The energy requirement for Ps formation is that $E_{\rm Ps}\geq 0$, i.e., that

$$E^b\geq E_L^i=I_i-6.8\ {\rm eV}-Q_{\rm Ps}+Q_+\ . \tag{A3}$$

This determines the lower limit of the Ore gap for energy level no. i. (Note that all through the present calculations we refer the energies to inside the crystal.) Finally, to compare with the experiments we subtract Q_+ from all positron kinetic energies. This means that experimentally the lower limits of the Ore gaps are independent of Q_+ while the upper limits are not [compare Eqs. (A3) with (5) and (6) in Sec. IV].

We estimate $Q_{\rm Ps}=-2\pm 1$ eV (Sec. IV A 4). A rough estimate of Q_+ is 1 eV (Ref. 35) (in agreement with measurements in this work which show Q_+ to be positive). Hence we allow Ps formation in the calculations at energies above $E_L^i=I_i-3.8$ eV. If the Ps has enough energy to split up again, the electron will subsequently be in the conduction band or at higher energies rather than in a valence band (as before Ps formation). Hence, the kinetic energy available to be shared between the positron and the electron is $E^b-E_i^*$ (this also shows that stable Ps is formed if $E^b<E_i^*$). Not knowing how this energy is partitioned among the two particles, we have chosen an even distribution (a denotes after):

$$E^a=(E^b-E_i^*)\mathscr{R}_1\ . \tag{A4}$$

In principle, Ps may split up if $E_{\rm Ps}$ is larger than the Ps binding energy in the crystal, i.e., if Ps is formed by a positron of energy E^b larger than E_i^*. However, it seems likely that also formation of Ps with a somewhat larger energy may result in stable Ps. One possibility could be that the formed Ps cools down to an energy in the stable regime by phonon scattering. Another possibility would be that the formed Ps travels a distance and then splits up, whereupon the positron and electron slow down by phonon scattering to thermal energies within each other's Coulomb attraction and finally recombine into stable Ps. A third possibility might be that Ps crosses the surface into the vacuum before splitting up. These considerations lead us to accept a higher threshold for stable Ps formation than $E^{\rm th}=E_i^*$, viz.

$$E^{\rm th}=E_i^*+\alpha\,|\,\mathscr{R}_2\,|\ ,$$

where $\mathscr{R}_2$ is a random number with a Gaussian distribution with the standard deviation 1. For the results shown below α was somewhat arbitrarily chosen to 4 eV.

No measurements have been performed of the excitation, ionization or the Ps formation cross sections. Hence, we have to estimate these. We do this by analogy with the results of Coleman *et al.*[63,64] for Ar, He, and Ne and by comparing these with the cross-section data for e^- slowing down in water by Turner *et al.*[45] In the energy range 10—15 eV (i.e., just above the lowest ionization energy in ice and water) the ratio between the excitation and ioniza-

tion cross sections, $\sigma^{\text{exc}}/\sigma^{\text{ion}}$, is very large for water (Ref. 45, Fig. 1). This is in agreement with the data for positrons[63] which show negligible ionization cross sections up to about 5 eV above the ionization energy. Above this the ionization cross sections increase approximately linearly with energy. Hence, we have chosen the σ_i^{ion} to be zero up to 5 eV above I_i and then to increase linearly with energy with a slope of 0.01 eV^{-1}. From Fig. 1 of Ref. 45 one can for $E \geq 17$ eV deduce the total excitation cross section, once σ_i^{ion} are known on assuming that positron and electron cross sections are the same. We have chosen to share this cross section equally between the energetically allowed excitations and to assume constancy below 17 eV.[63] Hence we obtain, e.g., $\sigma_1^{\text{exc}}=0.2$ up to about 22 eV, then it decreases and is const$=0.05$ above about 35 eV. [Since only relative values of the cross sections are important no units are used. Probably one unit is of the order of $5(\pi a_0^2)$ (Ref. 63 and 64)].

From a comparison of the cross sections in Ref. 63 and 64 (assuming that the Ps formation cross sections of Refs. 64 are correct), we estimate σ_i^{Ps} to be roughly equal to σ_i^{ion} at $\sim$50–100 eV and to rise steeply above the Ps formation threshold E_L^i. Hence we have chosen

$$\sigma_i^{\text{Ps}}=\begin{cases}0 & \text{for } E<E_L^i,\\ 1 & \text{for } E\geq E_L^i,\end{cases}$$

for $i=1,2,3$. The fourth broader band we have approximated by two, one with $I_4=27.5$ eV, one with $I_5=30.8$ eV, and with the cross sections rising linearly over the width of the band:

$$\sigma_4^{\text{Ps}}=\begin{cases}0.5[E-(27.5-3.8)]/3.3 & \text{for } 23.7\leq E<27.0 \text{ eV},\\ 0.5 & \text{for } 27.0 \text{ eV}\leq E,\end{cases}$$

and

$$\sigma_5^{\text{Ps}}=\begin{cases}0.5[E-(30.8-3.8)]/3.2 & \text{for } 27.0\leq E<30.2 \text{ eV},\\ 0.5 & \text{for } 30.2 \text{ eV}\leq E.\end{cases}$$

Finally, to account for the finite-energy resolution of the machine we have included an energy spread of FWHM equal to 1 eV on the nominal positron energies.

The result of the calculation is shown by curve d of Fig. 5. To illustrate the contributions to the total curve from the various electronic bands we have also plotted results of calculations if a) only one band were present (curve a) ($I_1=9.8$ eV. This result is very similar to that of Van House *et al.*[38]), two bands (curve b) (I_1 and $I_2=11.5$ eV), and three bands (curve c) (I_1, I_2, and $I_3=16.3$ eV).

Although there are deviations between the measured curve and the Monte Carlo simulation the similarity is striking. A number of assumptions and simplifications have been made, in the calculation, e.g., about cross sections and energy losses. However, if these parameters are varied within reasonable limits the curves obtained are qualitatively similar, although of course the details are varying. One exception to this is the assumption about the uniform energy distribution of the positron and electron kinetic energies after Ps splitup [Eq. (A4)]. If instead we assume that the two particles share the energy equally[39] [i.e., in Eq. (A4), $\mathscr{R}_1=0.5$] we obtain a curve with large variations also at the higher energies, rather than a constant one (see also Ref. 37). This is not in agreement with the experiments.

By carefully adjusting some of the parameters in the calculation we could no doubt calculate a curve almost identical to the experimental one. However, at the present stage this is probably proceeding too far. Later, more detailed experiments might form the basis for more refined Monte Carlo calculations from which information about positron and Ps scattering cross sections and energy losses can be deduced.

APPENDIX B: SIMULATION OF DOPPLER-BROADENING SPECTRA

The Doppler-broadening spectrum is measured in an energy interval of 14.6 keV ($=78$ channels $\times 187.6$ eV/channel) centered around the centroid of the spectrum. The spectrum contains several components:

$$B(E)=N_+^b+N_{p\text{-Ps}}^b+N_{p\text{-Ps}}^v+N_{o\text{-Ps}}^b+N_{o\text{-Ps}}^v+N_{\text{grid}}+N', \tag{B1}$$

where $+$ refers to free positrons, b and v to bulk and vacuum, respectively. N_{grid} is a contribution from annihilations in the accelerator grids of the machine,[24] and N' is an additional background, which may originate from various sources as discussed in Ref. 24. The intensities of these components are $I_i^j=\int N_i^j(E)dE$. The fraction of o-Ps in vacuum is given by Eq. (2). In the considered interval the energy distribution of the γ quanta from the 3γ decay of o-Ps in vacuum is roughly a square for $E\leq 511$ keV (for no "red shift," see below) and zero for larger E. Its area amounts to $\simeq 2.4\%$ of the total 3γ intensity. Hence we have for o-Ps and p-Ps in vacuum:

$$I_{o\text{-Ps}}^v=0.024p(E)d_o(E), \tag{B2}$$

$$I_{p\text{-Ps}}^v=\tfrac{1}{3}p(E)d_p(E), \tag{B3}$$

and in bulk:

$$I_{o\text{-Ps}}^b=p(E)[1-d_o(E)], \tag{B4}$$

$$I_{p\text{-Ps}}^b=\tfrac{1}{3}p(E)[1-d_p(E)], \tag{B5}$$

where

$$d_p(E)=[1+(E/E_p)^n]^{-1},$$

assuming an exponential positron penetration profile.

Since we have (Sec. III and Refs. 8 and 25)

$$A(E_i)^n=(D_{\text{Ps}}\tau_i)^{1/2},$$

we get

$$E_p=E_o(\tau_p/\tau_o)^{1/2n}.$$

For the positrons not forming Ps in the bulk, we have

$$I_+^b=1-4p(E)/3. \tag{B6}$$

Annihilation in the grids is estimated to contribute[24] $I_{\text{grid}}=0.06$, while a rough estimate[24] of I' is 0.05 (in the present study the exact values of these two terms are not important). The numerical values of the intensities as functions of E are derived using the fitted parameters E_o, n, β, and E_1 (Sec. III) inserted into Eqs. (2) and (B2)—(B6).

The shapes of the various components are in good approximations Gaussians, and their widths can be estimated from angular correlation curves for bulk ice.[12,43] Using the equivalence between Doppler-broadening and angular correlation curves (1 keV is equivalent to 3.914 mrad) and including a broadening of the components (the resolution of the Doppler broadening is 1.45 keV, that of the angular correlation is $\simeq 1$ mrad), we get for free e^+ FWHM equals 2.982 (ignoring a small contribution from 3γ decay) and for pick-off annihilation of o-Ps FWHM equals 3.071 keV. para-Ps in the bulk gives rise to three components,[12] viz. a narrow central peak from intrinsic annihilation (FWHM equals 1.472 keV, $I=0.633I^b_{p\text{-Ps}}$), a pick-off component (FWHM equals 3.071 keV, $I=0.092I^b_{p\text{-Ps}}$) and several "side peaks," that will be smeared out in a polycrystalline sample. We approximate this to a Gaussian (FWHM of 2.11 keV, $I=0.275I^b_{p\text{-Ps}}$). para-Ps in vacuum can only decay by intrinsic annihilation giving rise to a FWHM of 1.472 keV. However, if Ps leaves the sample surface (away from the detector) with a certain velocity, v_{Ps}, this gives rise to a red shift of this component (as well as of the vacuum ortho-Ps component) given by

$$\Delta E=511\frac{v_{\text{Ps}}}{c}\Big/\left[1+\frac{v_{\text{Ps}}}{c}\right]\text{(keV)}\,, \tag{B7}$$

where c is the velocity of light, and $v_{\text{Ps}}[=(E_{\text{Ps}}/m)^{1/2}]$ is assumed perpendicular to the surface. As an approximation we take the widths of the two last components in Eq. (B1) as FWHM equals 3.0 keV.

From these intensities and widths simulated Doppler-broadening curves were generated for various positron incident energies, E, and various E_{Ps}. The S parameter was determined as the area of the curve between -0.938 and $+0.938$ keV, and W as the sum of the areas between -5.440 and -1.876 keV and between 1.876 and 5.440 keV (zero being the curve centroid), both parameters normalized to the area of the whole curve. These windows are equivalent to the experimental ones (Sec. II). One set of simulated S and W parameters are shown in Fig. 9, and the curves which fit the experiments best are shown in Figs. 7 and 8.

*Present address: Metallurgy Department, Risø National Laboratory, DK-4000 Roskilde, Denmark.

[1]*Positrons in Solids,* edited by P. Hautojärvi (Springer, New York, 1979).

[2]*Positron Annihilation,* proceedings of the 5th International Conference on Positron Annihilation, Japan, 1979, edited by R. R. Hasiguti and K. Fujiwara (Japanese Institute of Metals, Sendai, Japan, 1979).

[3]*Positron Annihilation,* proceedings of the 6th International Conference on Positron Annihilation, Fort Worth, Texas, 1982, edited by P. G. Coleman, S. C. Sharma, and L. M. Diana (North-Holland, New York, 1982).

[4]*Positron Solid-State Physics,* proceedings of the "Enrico Fermi" School summer course on "Positrons in Solids," Varenna, Italy, 1981, edited by W. Brandt and A. Dupasquier (North-Holland, Amsterdam, 1983).

[5]T. C. Griffith and G. R. Heyland, Phys. Rep. C **39**, 169 (1978).

[6]K. G. Lynn, in *Positron Annihilation,* Ref. 2, p. 869.

[7]A. P. Mills, in *Positron Annihilation,* Ref. 3, p. 121; and in *Positron Solid-State Physics,* Ref. 4, p. 432.

[8]K. G. Lynn, in *Positron Solid-State Physics,* Ref. 4, p. 609.

[9]K. G. Lynn and H. Lutz, Rev. Sci. Instrum. **51**, 977 (1980).

[10]D. A. Fischer, K. G. Lynn, and W. E. Frieze, Phys. Rev. Lett. **50**, 1149 (1983).

[11]P. J. Schultz, K. G. Lynn, W. E. Frieze, and A. Vehanen, Phys. Rev. B **27**, 6626 (1983).

[12]O. E. Mogensen and M. Eldrup, J. Glaciol. **21**, 85 (1978); M. Eldrup, O. E. Mogensen, and J. H. Bilgram, *ibid.* **21**, 101 (1978); O. E. Mogensen and M. Eldrup, Risø Report No. 366, 1977 (unpublished), and references therein.

[13]M. Eldrup, in *Positron Annihiliation,* Ref. 3, p. 753; and in *Positron Solid-State Physics,* Ref. 4, p. 644.

[14]P. V. Hobbs, *Ice Physics* (Clarendon, Oxford, 1974).

[15]A. Dupasquier, in *Positron Solid-State Physics,* Ref. 4, p. 510.

[16]W. Brandt, Lett. Nuovo Cimento **33**, 499 (1982).

[17]H. J. Ache, in *Positron Annihilation,* Ref. 2, p. 31.

[18]O. E. Mogensen, J. Chem. Phys. **60**, 998 (1974); O. E. Mogensen, Appl. Phys. **6**, 315 (1975).

[19]O. E. Mogensen, in *Positron Annihilation,* Ref. 3, p. 763.

[20]R. Paulin, in *Positron Annihilation,* Ref. 2, p. 601.

[21]M. Eldrup, A. Vehanen, P. J. Schultz, and K. G. Lynn, Phys. Rev. Lett. **51**, 2007 (1983); **53**, 954 (1984).

[22]S. A. Rice, W. G. Madden, R. McGraw, M. G. Sceats, and M. S. Bergren, J. Glaciol. **21**, 509 (1978), and references therein; T. C. Sivakumar, S. A. Rice, and M. G. Sceats, J. Chem. Phys. **69**, 3468 (1978).

[23]V. I. Goldanskii, Atom. Energy Rev. **6**, 3 (1968).

[24]P. J. Schultz, K. G. Lynn, and H. H. Jorch, in notes from "Workshop on Slow Positrons in Surface Sciences," Finland 1984, Helsinki University of Technology, Laboratory of Physics Report No. 135 (unpublished).

[25]P. J. Schultz, K. G. Lynn, R. N. West, C. L. Snead, Jr., I. K. MacKenzie, and R. W. Hendricks, Phys. Rev. B **25**, 3637 (1982).

[26]H. H. Jorch, K. G. Lynn, and T. McMullen, Phys. Rev. B **30**, 93 (1984).

[27]K. G. Lynn and D. O. Welch, Phys. Rev. B **22**, 99 (1980).

[28]S. Valkealahti and R. M. Nieminen, Appl. Phys. A **32**, 95 (1983).

[29]P. J. Schultz, K. G. Lynn, and B. Nielsen, Phys. Rev. B **32**, 1369 (1985).

[30]J. Schou and H. Sørensen, J. Appl. Phys. **49**, 816 (1978); H. Sørensen and J. Schou, *ibid.* **49**, 5311 (1978).

[31]T. E. Everhardt and P. H. Hoff, J. Appl. Phys. **42**, 5837 (1971).

[32]A. Adams and P. K. Hansma, Phys. Rev. B **22**, 4528 (1980).

[33]H. Iskef, J. W. Cunningham, and D. E. Watt, Phys. Med. Biol. **28**, 535 (1983).

[34]A. P. Mills, Jr. and R. J. Wilson, Phys. Rev. A **26**, 490 (1982).
[35](a) M. Eldrup, Risø Report No. 254, 1971 (unpublished); (b) M. Eldrup, O. E. Mogensen, and G. Trumpy, J. Chem. Phys. **57**, 495 (1972).
[36]R. A. Rosenberg, V. Rehn, V. O. Jones, A. K. Green, C. C. Parks, G. Loubriel, and R. H. Stulen, Chem. Phys. Lett. **80**, 488 (1981).
[37]F. M. Jacobsen (unpublished).
[38]J. Van House, A. Rich, and P. W. Zitzewitz, Phys. Rev. Lett. **53**, 953 (1984).
[39]D. M. Schrader and R. E. Svetic, Can. J. Phys. **60**, 417 (1982).
[40]F. M. Jacobsen (private communication); O. E. Mogensen (private communication and unpublished).
[41]O. E. Mogensen and F. M. Jacobsen, Chem. Phys. **73**, 223 (1982).
[42]F. M. Jacobsen, in *Positron Scattering in Gases,* proceedings of the NATO Advanced Research Workshop, July, 1983, Egham, England, edited by J. W. Humbertson and M. R. C. McDowell (Plenum, New York, 1984), p. 85.
[43]R. J. Douglas, M. Eldrup, L. Lupton, and A. T. Stewart, in *Positron Annihilation,* Ref. 2, p. 621.
[44]J. M. Warman, M. P. de Hass, and J. B. Verberne, J. Phys. Chem. **84**, 1240 (1980).
[45]J. E. Turner, H. G. Paretzke, R. N. Hamm, H. A. Wright, and R. H. Ritchie, Radiat. Res. **92**, 47 (1982).
[46]T. L. Matskevich and E. G. Mikkailova, Phys. Tverd. Tela (Leningrad) **2**, 709 (1960) [Sov. Phys.—Solid State **2**, 655 (1960)].
[47]We use the term "Ps affinity" rather than "Ps work function" which would also be the correct terminology. However, the term "Ps work function" has been frequently used with a different, nonconventional, definition (Ref. 7).
[48]C. A. Murray and A. P. Mills, Jr., Solid State Commun. **34**, 789 (1980).
[49]D. W. Gidley, P. W. Zitzewitz, K. A. Marko, and A. Rich, Phys. Rev. Lett. **37**, 729 (1976).
[50]A. P. Mills, Jr., and L. N. Pfeiffer, Phys. Rev. Lett. **43**, 1961 (1979).
[51]A. P. Mills, Jr. and P. M. Platzman, Solid State Commun. **35**, 321 (1980).
[52]E. G. McRae, Rev. Mod. Phys. **51**, 54 (1979).
[53]M. Eldrup, A. Vehanen, P. J. Schultz, and K. G. Lynn, in notes from "Workshop on Slow Positrons in Surface Science," Finland, 1984, Helsinki University of Technology, Laboratory of Physics Report No. 135 (unpublished).
[54]K. F. Canter, in *Positron Annihilation,* Ref. 3, p. 138.
[55]A. Bar-nun, G. Herman, M. L. Rappaport, and Yu. Mekler, Surf. Sci. **150**, 143 (1985).
[56]J. Schou (private communication).
[57]M. Eldrup, J. Chem. Phys. **64**, 5283 (1976).
[58]N. J. Shevchik and W. Paul, J. Non-Cryst. Solids **16**, 55 (1974).
[59]P. D'Antonio and J. H. Konnert, Phys. Rev. Lett. **43**, 1161 (1979).
[60]E. Mayer and R. Pletzer, J. Chem. Phys. **80**, 2939 (1984).
[61]H. Ehrenreich and D. Turnbull, Comments Solid State Phys. **3**, 75 (1970).
[62]D. Grand and A. Bernas, Chem. Phys. Lett. **97**, 119 (1983).
[63]P. G. Coleman, J. T. Hutton, D. R. Cook, and C. A. Chandler, Can. J. Phys. **60**, 584 (1982).
[64]L. S. Fornari, L. M. Diana, and P. G. Coleman, Phys. Rev. Lett. **51**, 2276 (1983).